ESTIMATING ABOVEGROUND FOREST CARBON STOCKS USING MULTI-SENSOR SATELLITE DATA AND FIELD MEASUREMENTS IN THE PHILIPPINES

Jose Don T. De Alban[1,2,11,*], Rizza Karen A. Veridiano[3,4,11], Sean E.H. Pang[1], Mari Trix L. Estomata[5], Johanness Jamaludin[1], Angelica Kristina M. Jaojoco[6,11], Margie T. Parinas[7,10], Sheryl Rose C. Reyes[8,9,11], Roven D. Tumaneng[10,11], Akash Verma[1]

[1]Department of Biological Sciences, National University of Singapore, 117558 Singapore,
Email: s.pang@u.nus.edu; johanness.jamaludin@gmail.com; akash.verma@u.nus.edu
[2]Centre for Nature-based Climate Solutions, Department of Biological Sciences, National University of Singapore, 117558 Singapore,
Email: dbsjdtda@nus.edu.sg
[3]Center for Development Research, University of Bonn, 53113 Bonn, Germany;
[4]FORLIANCE GmbH, 53119 Bonn, Germany
Email: rizzakaren.veridiano@gmail.com);
[5]Deutsche Gesellschaft für Internationale Zusammenarbeit (GIZ) GmbH, Makati City, 1209, Philippines,
Email: trix.estomata@giz.de
[6]PS241 Consulting Inc., City of San Pedro, Laguna 4203, Philippines,
Email: angelicakv.monzon@gmail.com;
[7]National Mapping and Resource Information Authority, Fort Andres Bonifacio, Taguig City, 1634 Philippines,
Email: margieparinas@gmail.com;
[8]United Nations University - Institute for the Advanced Study of Sustainability, 5–53–70 Jingumae, Shibuya-ku, Tokyo 150-8925, Japan;
[9]Manila Observatory, Ateneo de Manila University Campus, Quezon City, 1108 Philippines,
Email: sreyes@observatory.ph
[10]Philippine Council for Industry, Energy, and Emerging Technology Research and Development – Department of Science and Technology, Bicutan, Taguig City, 1631 Philippines,
Email: rovendtumaneng@gmail.com;
[11]Fauna & Flora International, Philippines Programme, The David Attenborough Building, Pembroke Street, Cambridge, CB2 3QZ, United Kingdom

KEY WORDS: combined sensors, ALOS-PALSAR, Landsat, aboveground carbon stocks, forest inventory

ABSTRACT: Quantifying the amount of carbon stored in tropical forests is needed to inform climate mitigation mechanisms such as Reducing Emissions from Deforestation and Forest Degradation (REDD+). Remote sensing is a cost-effective tool to accurately estimate aboveground forest carbon stocks. Studies that use data from multiple sensors for estimating aboveground forest carbon, however, remain limited despite their tremendous potential. We estimated aboveground forest carbon stocks using multiple linear regression modeling between forest inventory data and satellite data, specifically L-band synthetic aperture radar (SAR) and Landsat, in three study sites in the Philippines. Models built using data from individual sensors versus combined multi-sensor data were assessed to determine which produced more accurate estimates of aboveground forest carbon. Subsequently, the accuracy of a global model developed from forest plot data across sites, was compared against site-specific models. Across sites, results showed that models using combined multi-sensor data performed better than those using individual sensors, with higher accuracies obtained for larger plot size (R^2=0.82-0.93; RMSE=27.20-42.92 Mg C ha^{-1}). Textural attributes made up the majority of predictors in these combined sensor models and contributed to improved accuracies and reduced uncertainties in carbon estimates. The global model did not perform better than site-specific models, regardless of sensor data or plot size, which suggests that the predictive power of the global model may be influenced by inherent site-specific variabilities (e.g., forest characteristics and forest inventory methods). Combining multi-sensor satellite data offers an improved approach for estimating aboveground forest carbon, with larger forest plot sizes contributing to this improvement, thus leading to higher accuracies and lower uncertainties for spatially explicit carbon mapping in dense tropical forest regions.

1. INTRODUCTION

The largest contributors to carbon dioxide (CO_2) emissions since the 1990s are deforestation and forest degradation (Gibbs et al., 2007; Pan et al., 2011). Due to the lack of forest plot data in South East Asia, estimates of carbon stocks and fluxes in tropical forests usually have large uncertainties. These uncertainties can lead to over- or underestimation of carbon emission reduction, which is crucial for carbon finance mechanisms (Pelletier et al., 2012).

A cost-effective way to measure and monitor spatially explicit estimates of aboveground forest carbon stocks (AFCS) is by calibrating spaceborne remote sensing data using forest inventory data (Rodríguez-Veiga et al., 2017). This method is usually based on a single sensor (Kajisa et al., 2009; Thapa et al., 2015a), but recent studies have increasingly focused on using multiple sensors to estimate AFCS (Santoro & Cartus, 2018). Nevertheless, AFCS estimates using combined sensors and forest inventory data are limited, especially in South East Asia. Furthermore, the effects of variable forest inventory design, forest type, and geography on the accuracy and precision of AFCS estimates are poorly understood (Dupuis et al., 2020; Miettinen et al., 2014).

This research pooled available forest inventory datasets with variable sampling designs to estimate AFCS in three sites in the Philippines. We developed multiple linear regression models between the satellite data (L-band SAR and Landsat) and forest inventory data for each site. Two research questions were pursued: 1) are estimates of AFCS from combined sensor data better than estimates from individual sensors, 2) will a "global"-model based on the pooled forest plot data from all three sites perform better than site-specific models?

2. STUDY SITES

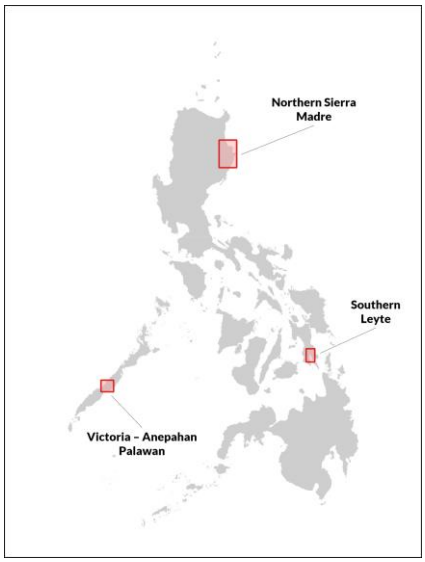

Figure 1. The location of the selected sites in the Philippines.

Aboveground forest carbon stocks were estimated for three study sites: (1) Northern Sierra Madre Natural Park (NSM) in northern Philippines (~17°18' N, 122°5' E) with a land area of 3,595 km^2, (2) Southern Leyte (SLY) in central-eastern Philippines (~10°50' N, 124°50' E) with a land area of 392 km^2, and (3) Victoria Anepahan Mountain range (VAM) in central-western Philippines (~9°19' N, 118°13' E) with a land area of 952 km^2. All three sites were identified as sub-national pilot demonstration sites under the Philippines National REDD+ Strategy (DENR – FMB, 2017, Philippine National REDD+ Strategy Team et al., 2011) (Fig. 1).

The three study sites contain mountainous terrains with tropical rainforest climate, except for VAM that has a tropical savanna climate (Peel et al., 2007). The selected study sites were either Key Biodiversity Areas or encompassed one – Mt. Nacolod in the case of SLY (Conservation International – Philippines et al., 2006; UNESCO World Heritage Centre, 2021). NSM is also the largest protected area in the country under the National Integrated Protected Areas System (Republic Act 9125 of 2001). The study areas host many endemic and globally threatened species; in SLY, recently discovered species of cloud forest frog (*Playtmantis navjoti*), and new island records such as Cebu cinnamon (*Cinnamomum cebuense*) and Little slaty flycatcher (*Ficedula basilanica*), among others (Diesmos et al., 2020; Mallari et al., 2013). Furthermore, these sites are the homes of several indigenous tribes such as the Agta or Dumagat (Minter et al., 2014) in NSM and the Pala'wan and Tagbanua (Eder, 1990) in VAM.

Deforestation and forest degradation at all three sites were driven by shifting cultivation, commercial agricultural production, illegal logging, and mining and road development (Carandang et al., 2013; Fernando et al., 2008). The topographic features of NSM made the site inaccessible, which helped keep its forests intact. Hence, NSM is one of the most extensive and contiguous remaining forests in the Philippines (Fernando et al., 2008; Whitmore, 1984). Meanwhile, the commercial logging ban by the Strategic Environmental Plan for Palawan Act (Republic Act 7611 of 1992) (Singh et al., 2017) has aided in preserving large tracts of forests in VAM.

3. DATA AND METHODS

3.1 Field Data

In all study sites, forest inventory data were collected including tree height, diameter at breast height (dbh), and species-level tree identification. Handheld global positioning system (GPS) receivers were used to record the geographic coordinates of all the sampling plots. Most of the plots in the three sites were distributed in both closed and open forests, but for SLY, some plots were in shrubs and wooded grassland.

For VAM, trees within the square plots were measured using two sampling methods: (i) nested sampling in 45 plots; and (ii) full sampling in 20 plots. For the nested sampling, trees were measured as follows: (a) all trees with 10-30cm dbh within a

20x20m square plot, (b) all trees >10cm dbh within a 50x20m plot, and (c) all trees >30cm dbh within the 50x50m plot. For the full sampling, all trees with dbh >5cm were measured within the 50x50m square plots. Four 50x50m square plots were arranged such that they were adjacent to each other to create a larger square plot with a total area of 1.0 ha (100x100m). Hence, five 1-hectare plots were randomly located in VAM (De Alban et al., 2014; Fauna & Flora International, 2014).

Table 1. Summary of forest inventory methods in the three sites.

Study Site	Sampling Design	Shape	Size (Area in ha)
NSM	Stratified systematic grid sampling	20-m radius nested circular plots	0.126
SLY	Stratified systematic grid sampling	12-m nested circular plots	0.045
VAM	Random Sampling	50x50m square plots	0.25

The 122 forest inventory plots for NSM were composed of nested circular plots with three radiuses – 4m, 14m and 20m. Within the smallest nested circular plot (4m), trees with 5-20cm dbh were measured, while in the 14m plots, trees with 20-50cm dbh; and in the biggest plot (20m), all trees with ≥ 50 cm dbh (Monzon et al., 2015). Like NSM, the forest inventory in SLY was also composed of nested circular plots but with different radiuses – 6m and 12m. Within the smaller plot (6m), trees with 6-20cm dbh were measured, while in the bigger plot (12m), trees with >20cm dbh. The forest inventory for SLY utilised a cluster approach such that each plot was in the four cardinal directions that were 50m from the center of the cluster. This cluster approach allowed the inventory of 382 circular plots for SLY (Schade & Ludwig, 2013).

To calculate carbon stocks, the biomass content of each tree measured in the field inventory was determined using Brown's equation (Eq. 1) (Brown, 1997; Pearson et al., 2005):

$$AGB = \exp [-2.289 + 2.649 \times (\ln D - 0.021) \times \ln D^2] \quad (1)$$

where *AGB* is the aboveground dry biomass (kg) and *D* is the diameter at breast height (dbh in cm). Since there is no country-specific allometric equation in the Philippines, Brown's equation was used to estimate biomass and because the equation was conservative in its various biomass and carbon estimations (Lasco et al., 2013; Lasco & Pulhin, 2009; Sullivan et al., 2017). Aboveground forest carbon stock (AFCS) is 50% of the dry biomass values (GOFC-GOLD, 2016) and extrapolated using an expansion factor (Eq. 2). The resulting forest carbon values (Mg C ha^{-1}) were used for succeeding regressions.

$$\text{Expansion Factor} = 10{,}000\ m^2 \div \text{area of plot} \quad (2)$$

3.2 Satellite Image Data

Advanced Land Observing Satellite (ALOS-1 and ALOS-2) Phased Array L-band Synthetic Aperture Radar (PALSAR-1 and PALSAR-2) global 25-meter dual-polarisation mosaics (2007-2010 and 2015-2017, respectively) and Tier 1 calibrated top-of-the-atmosphere reflectance Landsat image collection that were available at the time of processing in the Google Earth Engine (GEE) Data Catalog (https://explorer.earthengine.google.com) were used for this study. GEE, a cloud-based geospatial analysis platform (Gorelick et al., 2017), was used to implement the mosaic data extraction, image stacking, and majority of the image processing to prepare the inputs to the modeling.

Prior to the calculation of indices and texture measures, the initial radar image stack had 14 layers corresponding to the HH (horizontal transmit – horizontal receive) and HV (horizontal transmit – vertical receive) polarisation channels of each available year, which were exported from GEE and imported into the European Space Agency's Sentinel Application Platform (SNAP) Toolbox (https://step.esa.int/main/toolboxes/snap/) to implement a multi-temporal speckle filtering process. A Lee Sigma multi-temporal speckle filter was employed, which enables filtering without compromising spatial resolution and achieving better radiometric resolution (Quegan & Yu, 2001). The multi-temporal speckle-filtered HH- and HV-polarised images were converted into normalised radar cross-sections using the equation from Shimada et al. (2009) and were used to generate the six radar indices.

For the optical imagery, using the best-available-pixel compositing method (Griffiths et al., 2013; White et al., 2014), near-cloud-free 30-meter Landsat composites for each study site were generated from available satellite images across all missions.

Table 2. Summary of combined L-band SAR and Landsat image stacks per study site.

Sensor	NSM	SLY	VAM
L-band SAR (88 layers)	ALOS-2/PALSAR-2 - 2015 mosaic - 2 polarisations - 6 indices - 80 GLCM textures	ALOS/PALSAR - 010 mosaic - polarisations - indices - 0 GLCM textures	ALOS/PALSAR - 010 mosaic - polarisations - indices - 0 GLCM textures
Landsat (252	L7 ETM+ / L8 OLI - 2014 composite	L5 TM / L7 ETM+ - 011–2012 composite	L7 ETM+ / L8 OLI - 013 composite

layers)	- 7 bands - 5 indices - 240 GLCM textures	- bands - indices - 40 GLCM textures	- bands - indices - 40 GLCM textures

Second-order texture measures from the radar (HH and HV-polarised sigma nought) and optical (blue, green, red, near-infrared and two shortwave infrared bands) images were calculated using the GEE platform. Grey-Level Co-occurrence Matrices (GLCM) were calculated to derive the eight texture measures for each SAR and each Landsat image.

Table 3. Summary of all radar and optical indices and GLCM textures.

	Band	**Source**
Radar	HH over HV (SAR Index 1 or HHoHV) HV over HH (SAR Index 2 or HVoHH) SAR Average (AVE) SAR Difference (DIF) Normalised Difference Index (NDI; also known as the Forest Degradation Index, RFDI) Normalised Index (NLI)	 (Almeida-Filho et al., 2009) (Li et al., 2012)
Optical	Enhanced Vegetation Index (EVI) Land Surface Water Index (LSWI) Normalised Difference Tillage Index (NDTI) Normalised Difference Vegetation Index (NDVI) Soil-Adjusted Total Vegetation Index (SATVI) Enhanced Vegetation Index (EVI)	(Huete et al., 1997, 2002) (Gao, 1996; Jurgens, 1997) (van Deventer et al., 1997) (Rouse et al., 1974; Tucker, 1979) (Hagen et al., 2012; Marsett et al., 2006) (Huete et al., 1997, 2002)
GLCM Textures	Contrast (CON), Dissimilarity (DIS), Inverse difference moment (IDM), Angular second moment (ASM), Entropy (ENT), Mean (AVG), Correlation (COR), Variance (VAR)	(Haralick et al., 1973)

Image statistics from all layers of the final image stacks were extracted onto each forest plot polygon. For each site, three input datasets including the total forest carbon estimate per plot were assembled as follows: PALSAR-only, Landsat-only, and combined PALSAR and Landsat variables. The R software environment (R Core Team, 2020) was used to perform data handling, model calibration and validation, and creation of plots.

3.3 Modeling

A multiple linear regression approach was adopted to model the relationship between extracted sensor variables from radar and optical satellite data (predictors) and field-measured aboveground forest carbon (response). A total of 12 models were developed – three sensor data types for each study site, and additional three more for VAM's full sampling plots. Model calibration was done stepwise to determine the combination of variables with the greatest explanatory power and minimal multicollinearity. The predictor with the highest R-squared (R^2) to the response variable was added first. Subsequent steps involved including the predictor resulting in the lowest p-value (F-test) and removing any non-significant predictors (p-value > 0.05, T-test); steps end when the added predictor was also removed. The fit of the final model was then evaluated using R^2 and Root Mean Square Error (RMSE).

Model performance was evaluated using the 10-fold cross-validation strategy. Three metrics of model performance were calculated: R^2, RMSE, and the Kling-Gupta Efficiency (KGE; Eq. 3) (Gupta & Kling, 2011). KGE was defined as

$$KGE = 1 - \sqrt{(r-1)^2 + (\alpha-1)^2 + (\beta-1)^2} \quad (3)$$

where *r* is the correlation, α the ratio of means, β the ratio of standard deviations, between observed and predicted AFCS values. Accurate models yield high R^2 and KGE, while lower RMSE indicates less uncertainties for the model's carbon estimates.

'Global' models were calibrated and evaluated similarly to site-specific models but used the field-measured aboveground forest carbon from all three sites. For comparability of model performance scores, global models were evaluated with the same testing data used to evaluate the site-specific models (i.e., each testing fold).

4. RESULTS

Four forest plots in NSM and SLY had very high AFCS (>1000 Mg C ha^{-1}), but most forest plots had carbon values of 0–400 Mg C ha^{-1}.

Table 4. Summary of AFCS in forest inventory plots

Site	**AFCS (Mg C ha^{-1})**

	Mean	Range
NSM	361.40	100–400
SLY	154.24	0–200
VAM (nested)	213.01	200–300
VAM (full)	237.44	200–300

The combined sensor models outperformed the models calibrated using individual sensors, for all study sites (higher R^2 and lower RMSE) (Fig. 2). Although for NSM and SLY, their models yielded relatively low R^2 and high RMSE values, even against the individual sensor models of VAM. SLY's best model had an R^2 value lower than the best model for NSM, which had a plot size thrice as big as the plots of SLY (Table 5). The RMSE for SLY was also relatively lower than that of NSM, but relative to the dominant range of carbon values in the two sites, the RMSE is still high. The combined sensor models for VAM (nested and full sampling) produced high R^2 (0.82 and 0.93) and low RMSE (42.92 Mg C ha^{-1} and 27.20 Mg C ha^{-1}). The combined sensor global models also outperformed the global models calibrated using individual sensors. However, compared to all the site-specific models using combined sensors, the best global model still performed poorly.

Table 5. Model calibration results for models applied at site level and across all study sites to estimate aboveground forest carbon using combined sensor data. Metric scores show R^2 and RMSE (in Mg C ha^{-1}) for evaluating model fit.

Model	Model Equation	R^2	RMSE (Mg C ha^{-1})
NSM (Nested; 0.126 ha)			
NSM-Model-3	–47341.27 + 2195252.90**HH_K5_ASM** – 1580.46**B3_K11_ENT** + 1369.68**B3_K9_ENT** – 537.82**B4_K5_COR** – 431372.28**HV_K5_ASM** – 694.26**HV_K7_COR** – 32759.79**HH_K5_IDM** – 2132.00**B6_K7_IDM** + 7.99**B3_K5_VAR** + 483.74**B2_K7_COR** – 3.43**B4_K11_VAR**	0.39	300.87
SLY (Nested; 0.045 ha)			
SLY-Model-3	1372.19 + 0.03**HV_K11_AVG** – 254.46**B7_K7_COR** + 2.01**HV_K11_VAR** + 13.43**B4_K5_AVG** – 19.17**B6_K11_DIS** + 0.04**B5_K9_VAR** + 0.07**NLI** – 6.015**B3_K3_AVG** + 798.24**LSWI** + 109.14**B6_K3_COR** – 11397.39**B7_K7_ASM** – 5.62**B3_K11_AVG** – 14.78**B2_K5_DIS**	0.28	177.89
VAM (Nested; 0.25 ha)			
VAM-Model-3	–15768.63 + 1.91**B7_K11_VAR** + 0.10**HV_K11_AVG** + 135.72**B4_K3_IDM** + 5030.31**HH_K5_ENT** + 1782.07**B5_K11_IDM** + 0.15**HH_K7_DIS** – 0.0002**HV_K11_CON** + 0.35**B6_K11_VAR** – 132.85**B2_K3_COR** + 466.37**B6_K3_IDM** – 0.05**DIF** + 224.85**B6_K5_COR** – 1133.08**B6_K9_IDM** – 119.39**B5_K5_COR** + 0.33**HH_K11_DIS** + 0.50**B2_K7_CON** + 2447.94**B3_K11_ASM**	0.82	42.92
VAM (Full; 0.25 ha)			
VAM-Model-6	3267.79 + 0.03**AVE** + 369350.37**HV_K3_IDM** – 597.09**B7_K11_COR** – 59248.92**B6_K5_ASM** + 28513.65**HV_K5_IDM** – 776.84**HH_K11_COR** – 298.02**B3_K3_ENT** – 114.38**B7_K3_COR** + 286.63**B5_K7_COR** – 628.06**SATVI** – 3757.41**B4_K7_ASM**	0.93	27.20
Across all study sites			
Global-Model-3	–75859.24 – 27.12**B6_K11_DIS** + 10.47**B5_K7_DIS** – 131.16**B2_K11_ENT** – 734.06**NDTI** + 110.06**B2_K3_ENT** – 142.04**HV_K3_COR** + 13290.14**HH_K5_IDM** + 14979.35**HH_K11_ENT** – 3912.62**HH_K3_IDM** – 27249.85**HV_K3_ASM** + 297.23**B2_K11_COR** – 219.31**B4_K7_COR** + 26.81**HVg0** – 0.04**DIF** – 179.36**B3_K3_IDM**	0.24	230.61

In addition to the acronyms of the indices and texture measures listed in Table 3, additional acronyms of predictor variables used in Table 5 area as follows: (1) Predictors related to SAR data include horizontal transmit – vertical receive (HV), horizontal transmit – horizontal receive (HH), HH or HV backscatter coefficient (HHg0, HVg0); (2) Predictors related to Landsat data include blue (B2), green (B3), red (B4), near-infrared (B5), shortwave infrared 1 (B6), and shortwave infrared 2 (B7). The neighbourhood kernel/window sizes of the texture measures range from 3x3 (K3), 5x5 (K5), 7x7 (K7), 9x9 (K9), until 11x11 (K11).

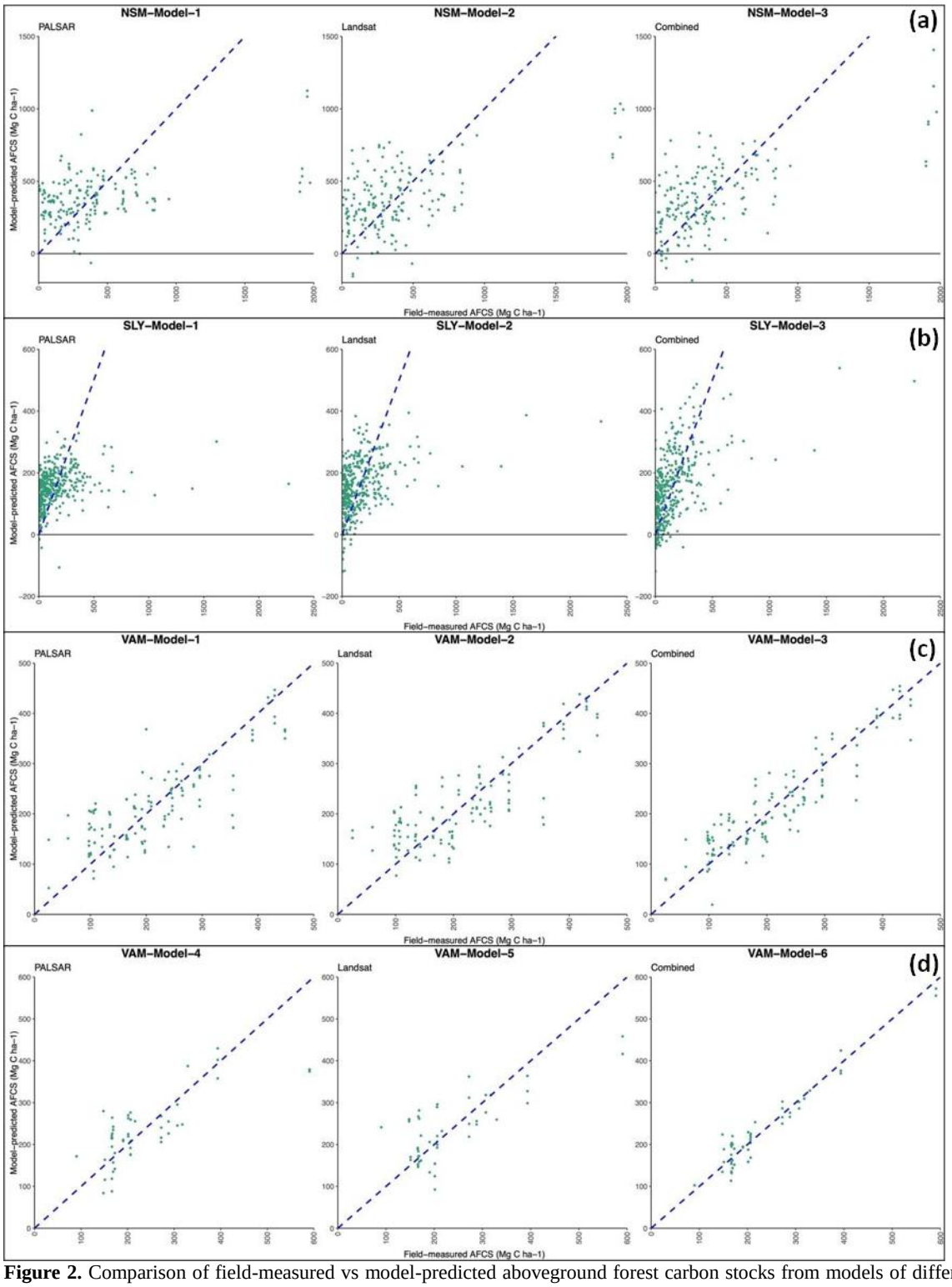

Figure 2. Comparison of field-measured vs model-predicted aboveground forest carbon stocks from models of different sensor data types in (a) NSM (nested sampling plots), (b) in SLY (nested sampling plots), (c) VAM (nested sampling plots) and (d) VAM (full sampling plots).

After using a 10-fold cross validation strategy, the results of the model evaluation for combined sensor models were mostly lower than the calibration results. For NSM and VAM (both nested and full sampling), the evaluation R^2 was lower than the calibration R^2, while evaluation RMSEs were higher than calibration RMSEs, which indicated a decrease in model accuracy and model uncertainty, respectively. NSM-Model-3 had an R^2 of 0.25±0.16 and KGE of 0.06±0.31, and RMSE of 349.68±137.82 Mg C ha^{-1}. For VAM, VAM-Model-3 (nested sampling) had an R^2 of 0.50±0.31, KGE of 0.50±0.33, and RMSE of 57.21±8.19 Mg C ha^{-1}, whereas VAM-Model-6 (full sampling) had an R^2 of 0.62±0.36, KGE of –3.70±13.05, and RMSE of 36.57±20.14 Mg C ha^{-1}. While SLY and the global models had higher evaluation R^2 than calibration R^2 and lower evaluation RMSEs than calibration RMSEs, their R^2 and KGE values were still lower than that of VAM's models with

nested sampling plots. SLY's model with best evaluation results was SLY-Model-3 with R^2 of 0.32±0.12, KGE of 0.32±0.20 and RMSE of 172.92±78.33 Mg C ha^{-1}. Global-Model-3 had an R^2 of 0.21±0.26, KGE of –1.17±6.17 and RMSE of 188.78±137.25 Mg C ha^{-1}.

5. DISCUSSION

This study demonstrated that combined L-band SAR and optical data improved model estimations of AFCS in the Philippines, as also demonstrated by other studies in South East Asia (Cutler et al., 2012; Lang et al., 2021; Pham et al., 2020). Previous studies also showed how model accuracies were improved and uncertainties reduced when textural attributes were included as model predictors in estimating aboveground forest carbon in optical (Kelsey & Neff, 2014) and SAR data (Thapa et al., 2015a; Thapa et al., 2016). The aggregation process of the neighborhood sizes (large kernel sizes) used in texture analysis might be the reason why the performance of models improved when textural attributes were considered. The neighborhood/kernel-based aggregation of textural attributes may explain improvements in model performance. This might also be addressing a) possible positional errors between satellite and forest plot data, b) speckle noise in SAR data, and c) saturation problems in L-band SAR for biomass estimation in dense tropical forests. L-band SAR textures did not only help identify changes in canopy structure in regenerating tropical forests (Luckman et al., 1997), but also captured the spatial variation of tropical forest canopy structure as well as the increase in roughness and complexity of maturing tropical forests (Kuplich et al., 2005). Optical data textures correlated with tropical forest biomass and improved AFCS estimation (Eckert, 2012; Lu, 2005). Hence, it would be crucial to utilise textural attributes from multiple sensors to accurately estimate AFCS and to monitor carbon fluxes in areas with forest disturbances like in South East Asia (Kelsey & Neff, 2014).

All site-specific models using combined sensor data outperformed the global combined sensor model, which aligned with previous studies (Cutler et al., 2012; Foody et al., 2003). The global model in this study did not perform very well compared to Cutler et al.'s (2012) global model, possibly due to similar forest characteristics between the three inter-country study sites. This suggests that using pooled datasets from various forest inventories, even with combined sensor data, could generate unreliable model estimates at larger scales (i.e., country, or regional) if forest characteristics varied substantially across forest landscapes.

We demonstrate that better remotely sensed AFCS estimates can be achieved using larger forest inventory plot sizes. Despite having fewer large plots (45 nested, 20 full sampling plots) for VAM, better carbon estimates were achieved compared to the hundreds of smaller plots in NSM (122) and SLY (382), possibly because smaller plots are limited by their ability to capture the spatial heterogeneity of forest characteristics. Larger plots covered more neighboring pixels, which did not only enable it to account for the spatially varying characteristics of dense tropical forests (Asner et al., 2010) but also minimised plot-edge effects, where uncertainties arise due to the inclusion/exclusion of a tree in forest inventories (Packalen et al., 2015; Pascual et al., 2019).

Full tree sampling of large plots in VAM produced better model-predicted AFCS estimates than the nested plots. This was expected since full sampling did not rely on extrapolations of tree biomass calculations for the plot, as it did for nested plots, which introduced the uncertainty into the calculations. These findings were consistent with other studies such as that in Indonesia where all trees larger than 5 cm were measured in one-hectare plots and obtained good model performance (R^2 0.73–0.87 and RMSE 17.4–30.9 Mg C ha^{-1}) (Thapa et al., 2016; Thapa et al., 2015a; Thapa et al., 2015b), while in Malaysia, 0.126-ha circular nested sampling plots were used and obtained low model performances using L-band SAR only (R^2 0.3541; RMSE 116.91 Mg C ha^{-1}) or using multi-frequency SAR data (R^2 0.356; RMSE 98.41 Mg C ha^{-1}) (Omar et al., 2017; Omar & Misman, 2018).

Spatially explicit forest carbon datasets can provide reliable estimates for nature-based solutions like the United Nations REDD+ mechanism (UNDP, 2021). Statistics of biomass stocks of different forest types are obtained using conventional forest plot networks that utilise nested sampling approaches (IPCC, 2006; Walker et al., 2012) and are not designed to capture changes that could affect carbon stocks differently (Avitabile et al., 2011). However, if the intention is to quantify AFCS using field-calibrated remote sensing data, then field measurements from conventional forest inventories will yield unreliable model estimates of AFCS, even with combined sensor data.

The possible sources of uncertainties in this study's AFCS estimates may be from the following: 1) degraded positional accuracies from handheld GPS receivers under dense forest canopies during forest inventory, 2) a generic tree allometric model (Brown, 1997), 3) temporal mismatch between dates of field data collection and satellite image composites, and 4) the large difference between the pixel resolution of the remote sensing data and field measurement plots (Saatchi et al., 2011).

6. CONCLUSIONS

This study showed that more accurate AFCS estimates can be derived from combined SAR and optical remote sensing data, instead of estimating from individual sensors. Model accuracy improved and uncertainty estimates were reduced when combined sensor textural attributes were utilised. Better AFCS estimates were produced from large, fully sampled plots

compared to small, nested plots. Site-specific models produced better estimates than global models despite using combined sensors. The ongoing satellite constellations and future satellite missions could provide opportunities to further improve aboveground forest carbon mapping, which is important for nature-based solutions to better contribute to mitigating climate change such as REDD+ mechanisms that need improved accuracies and reduced uncertainties to verify spatially explicit carbon maps in dense tropical forest regions.

ACKNOWLEDGEMENTS:

This work was undertaken within the framework of the JAXA Kyoto & Carbon Initiative (Phase 3 and Phase 4). The authors acknowledge the following organisations for the provision of forest inventory data: i) NSM – Chemonics International and the Forest Management Bureau of the Department of Environment and Natural Resources, funded by United States Agency for International Development, ii) VAM – Non-Timber Forest Products-Task Force, Fauna & Flora International Philippines, Environmental Legal Assistance Center, Institute for the Development of Educational and Ecological Alternatives, Nagkakaisang mga Tribu ng Palawan, and the Local Government of Quezon, Palawan funded by both European Union and International Union for the Conservation of Nature-Ecosystem Alliance, iii) SLY – Deutsche Gesellschaft für Internationale Zusammenarbeit (GIZ) GmbH and the Forest Management Bureau of the Department of Environment and Natural Resources, funded by the German Federal Ministry for the Environment, Nature Conservation, Building and Nuclear Safety (BMUB) under its International Climate Initiative.

REFERENCES:

Almeida-Filho, R., Shimabukuro, Y. E., Rosenqvist, A., & Sánchez, G. A. (2009). Using dual-polarized ALOS PALSAR data for detecting new fronts of deforestation in the Brazilian Amazônia. International Journal of Remote Sensing, 30(14), 3735–3743.

Asner, G. P., Powell, G. V. N., Mascaro, J., Knapp, D. E., Clark, J. K., Jacobson, J., Kennedy-Bowdoin, T., Balaji, A., Paez-Acosta, G., Victoria, E., Secada, L., Valqui, M., & Hughes, R. F. (2010). High-resolution forest carbon stocks and emissions in the Amazon. Proceedings of the National Academy of Sciences, 107(38), 16738–16742.

Avitabile, V., Herold, M., Henry, M., & Schmullius, C. (2011). Mapping biomass with remote sensing: A comparison of methods for the case study of Uganda. Carbon Balance and Management, 6(1), 7.

Brown, S. (1997). Estimating Biomass and Biomass Change of Tropical Forests: A Primer. Food and Agriculture Organization of the United Nations. http://www.fao.org/docrep/w4095e/w4095e00.HTM

Carandang, A. P., Bugayong, L. A., Dolom, P. C., Garcia, L. N., Villanueva, Ma. M. B., Espiritu, N. O., & Forest Development Center, University of the Philippines Los Banos. (2013). Analysis of Key Drivers of Deforestation and Forest Degradation in the Philippines (p. 128). Deutsche Gesellschaft für Internationale Zusammenarbeit (GIZ) GmbH.

Conservation International – Philippines, Protected Areas and Wildlife Bureau, & Haribon Foundation. (2006). Priority Sites for Conservation in the Philippines: Key Biodiversity Areas. Conservation International - Philippines.

Cutler, M. E. J., Boyd, D. S., Foody, G. M., & Vetrivel, A. (2012). Estimating tropical forest biomass with a combination of SAR image texture and Landsat TM data: An assessment of predictions between regions. ISPRS Journal of Photogrammetry and Remote Sensing, 70, 66–77.

De Alban, J. D. T., Monzon, A. K. V., Veridiano, R. K. A., Rico, E. L. B., Pales, J. R., Tumaneng, R. D., Parinas, M. T., & Paringit, E. C. (2014). Forest change detection and biomass estimation using ALOS/PALSAR data in support of REDD+ readiness activities in Palawan, Philippines (ALOS K&C Science Report – Phase 3, p. 16). ALOS Kyoto & Carbon Initiative.

DENR – FMB. (2017). Update of the Philippine National REDD-plus Strategy. Deutsche Gesellschaft für Internationale Zusammenarbeit (GIZ) GmbH.

Diesmos, A. C., Scheffers, B. R., Mallari, N. A. D., Siler, C. D., & Brown, R. M. (2020). A new forest frog of the genus Platymantis (Amphibia: Anura: Ceratobatrachidae: subgenus Tirahanulap) from Leyte and Samar islands, eastern Philippines. Zootaxa, 4830(3), 573–591.

Dupuis, C., Lejeune, P., Michez, A., & Fayolle, A. (2020). How Can Remote Sensing Help Monitor Tropical Moist Forest Degradation? — A Systematic Review. Remote Sensing, 12(7), 1087.

Eckert, S. (2012). Improved Forest Biomass and Carbon Estimations Using Texture Measures from WorldView-2 Satellite Data. Remote Sensing, 4(4), 810–829.

Eder, J. F. (1990). Deforestation and detribalization in the Philippines: The Palawan case. Population and Environment, 12(2), 99–115.

Fauna & Flora International. (2014). Carbon Stock Assessment Manual (p. 22). Fauna & Flora International - Philippines Programme.

Fernando, E. S., Suh, M. H., Lee, J., & Lee, D. K. (2008). Forest Formations of the Philippines. ASEAN-Korea Environmental Cooperation Unit (AKECU).

Foody, G. M., Boyd, D. S., & Cutler, M. E. J. (2003). Predictive relations of tropical forest biomass from Landsat TM data and their transferability between regions. Remote Sensing of Environment, 85(4), 463–474.

Gao, B. (1996). NDWI—A normalized difference water index for remote sensing of vegetation liquid water from space. Remote Sensing of Environment, 58(3), 257–266.

Gibbs, H. K., Brown, S., Niles, J. O., & Foley, J. A. (2007). Monitoring and estimating tropical forest carbon stocks: Making REDD a reality. Environmental Research Letters, 2(4), 045023.

GOFC-GOLD. (2016). A Sourcebook of Methods and Procedures for Monitoring and Reporting Anthropogenic Greenhouse Gas Emissions and Removals Associated with Deforestation, Gains and Losses of Carbon Stocks in Forests Remaining Forests, and Forestation (No. COP22-1). GOFC-GOLD Land Cover Project Office, Wageningen University.

Gorelick, N., Hancher, M., Dixon, M., Ilyushchenko, S., Thau, D., & Moore, R. (2017). Google Earth Engine: Planetary-scale geospatial analysis for everyone. Remote Sensing of Environment, 202, 18–27.

Griffiths, P., Linden, S. van der, Kuemmerle, T., & Hostert, P. (2013). A pixel-based Landsat compositing algorithm for large area land cover mapping. IEEE Journal of Selected Topics in Applied Earth Observations and Remote Sensing, 6(5), 2088–2101.

Gupta, H. V., & Kling, H. (2011). On typical range, sensitivity, and normalization of Mean Squared Error and Nash-Sutcliffe Efficiency type metrics: TECHNICAL NOTE. Water Resources Research, 47(10).

Hagen, S. C., Heilman, P., Marsett, R., Torbick, N., Salas, W., van Ravensway, J., & Qi, J. (2012). Mapping total vegetation cover across western rangelands with Moderate-Resolution Imaging Spectroradiometer data. Rangeland Ecology & Management, 65(5), 456–467.

Haralick, R. M., Shanmugam, K., & Dinstein, I. (1973). Textural features for image classification. IEEE Transactions on Systems, Man, and Cybernetics, 3(6), 610–621.

Huete, A. R., Didan, K., Miura, T., Rodriguez, E. P., Gao, X., & Ferreira, L. G. (2002). Overview of the radiometric and biophysical performance of the MODIS vegetation indices. Remote Sensing of Environment, 83(1), 195–213.

Huete, A. R., Liu, H. Q., Batchily, K., & van Leeuwen, W. (1997). A comparison of vegetation indices over a global set of TM images for EOS-MODIS. Remote Sensing of Environment, 59(3), 440–451.

IPCC. (2006). 2006 IPCC Guidelines for National Greenhouse Gas Inventories—Volume 4: Agriculture, Forestry, and Other Land Uses. International Panel on Climate Change.

Jurgens, C. (1997). The modified normalized difference vegetation index (mNDVI) a new index to determine frost damages in agriculture based on Landsat TM data. International Journal of Remote Sensing, 18(17), 3583–3594.

Kajisa, T., Murakami, T., Mizoue, N., Top, N., & Yoshida, S. (2009). Object-based forest biomass estimation using Landsat ETM+ in Kampong Thom Province, Cambodia. Journal of Forest Research, 14(4), 203–211.

Kelsey, K., & Neff, J. (2014). Estimates of Aboveground Biomass from Texture Analysis of Landsat Imagery. Remote Sensing, 6(7), 6407–6422.

Kuplich, T. M., Curran, P. J., & Atkinson, P. M. (2005). Relating SAR image texture to the biomass of regenerating tropical forests. International Journal of Remote Sensing, 26(21), 4829–4854.

Lang, N., Schindler, K., & Wegner, J. D. (2021). High carbon stock mapping at large scale with optical satellite imagery and spaceborne LIDAR. ArXiv:2107.07431 [Cs]. http://arxiv.org/abs/2107.07431

Lasco, R. D., & Pulhin, F. B. (2009). Carbon budgets of forest ecosystems in the Philippines. Journal of Environmental Science and Management, 12(1), 1–13.

Lasco, R. D., Veridiano, R. K. A., Habito, M., & Pulhin, F. B. (2013). Reducing emissions from deforestation and forest degradation plus (REDD+) in the Philippines: Will it make a difference in financing forest development? Mitigation and Adaptation Strategies for Global Change, 18(8), 1109–1124.

Li, G., Lu, D., Moran, E., Dutra, L., & Batistella, M. (2012). A comparative analysis of ALOS PALSAR L-band and RADARSAT-2 C-band data for land-cover classification in a tropical moist region. ISPRS Journal of Photogrammetry and Remote Sensing, 70, 26–38.

Lu, D. (2005). Aboveground biomass estimation using Landsat TM data in the Brazilian Amazon. International Journal of Remote Sensing, 26(12), 2509–2525.

Luckman, A., Baker, J., & Kuplich, T. M. (1997). A Study of the Relationship between Radar Baekseatter and Regenerating Tropical Forest Biomass for Spaeeborne SAR Instruments. 13.

Mallari, N. A., Rico, E. L., De Alban, J. D. T., Diesmos, A., Altamirano, R. A., Puna, N., Supsup, C., Ledesma, M., Nuevo-Diego, C. E., Lillo, E., Monzon, A. K., Veridiano, R. K., Wenceslao, J., Tablazon, D., Masigan, J. P., Lorca, R. N., Tumaneng, R., Pales, J. R., Guinto, A. F., … Musa, M. (2013). Biodiversity baseline assessment in the REDD+ pilot and key biodiversity area in Mt Nacolod, Southern Leyte. Deutsche Gesellschaft für Internationale Zusammenarbeit (GIZ) GmbH.

Marsett, R. C., Qi, J., Heilman, P., Biedenbender, S. H., Carolyn Watson, M., Amer, S., Weltz, M., Goodrich, D., & Marsett, R. (2006). Remote sensing for grassland management in the arid Southwest. Rangeland Ecology & Management, 59(5), 530–540.

Miettinen, J., Stibig, H.-J., & Achard, F. (2014). Remote sensing of forest degradation in Southeast Asia—Aiming for a regional view through 5–30 m satellite data. Global Ecology and Conservation, 2, 24–36.

Minter, T., Ploeg, J. van der, Pedrablanca, M., Sunderland, T., & Persoon, G. A. (2014). Limits to indigenous participation: The Agta and the Northern Sierra Madre Natural Park, the Philippines. Human Ecology, 42(5), 769–778.

Omar, H., & Misman, M. A. (2018). Time-series maps of aboveground biomass in dipterocarps forests of Malaysia from PALSAR and PALSAR-2 polarimetric data. Carbon Balance and Management, 13(1), 19.

Omar, H., Misman, M. A., & Kassim, A. R. (2017). Synergetic of PALSAR-2 and Sentinel-1A SAR Polarimetry for Retrieving Aboveground Biomass in Dipterocarp Forest of Malaysia. 20.

Packalen, P., Strunk, J. L., Pitkanen, J. A., Temesgen, H., & Maltamo, M. (2015). Edge-Tree Correction for Predicting Forest Inventory Attributes Using Area-Based Approach With Airborne Laser Scanning. IEEE Journal of Selected Topics in Applied Earth Observations and Remote Sensing, 8(3), 1274–1280.

Pan, Y., Birdsey, R. A., Fang, J., Houghton, R., Kauppi, P. E., Kurz, W. A., Phillips, O. L., Shvidenko, A., Lewis, S. L., Canadell, J. G., Ciais, P., Jackson, R. B., Pacala, S. W., McGuire, A. D., Piao, S., Rautiainen, A., Sitch, S., & Hayes, D. (2011). A Large and Persistent Carbon Sink in the World's Forests. Science, 333(6045), 988–993.

Pascual, A., Pukkala, T., de Miguel, S., Pesonen, A., & Packalen, P. (2019). Influence of size and shape of forest inventory units on the layout of harvest blocks in numerical forest planning. European Journal of Forest Research, 138(1), 111–123.

Peel, M. C., Finlayson, B. L., & McMahon, T. A. (2007). Updated world map of the Köppen-Geiger climate classification. Hydrology and Earth System Sciences, 11(5), 1633–1644.

Pelletier, J., Kirby, K. R., & Potvin, C. (2012). Significance of carbon stock uncertainties on emission reductions from deforestation and forest degradation in developing countries. Forest Policy and Economics, 24, 3–11.

Pham, T. D., Le, N. N., Ha, N. T., Nguyen, L. V., Xia, J., Yokoya, N., To, T. T., Trinh, H. X., Kieu, L. Q., & Takeuchi, W. (2020). Estimating Mangrove Above-Ground Biomass Using Extreme Gradient Boosting Decision Trees Algorithm with Fused Sentinel-2 and ALOS-2 PALSAR-2 Data in Can Gio Biosphere Reserve, Vietnam. Remote Sensing, 12(5), 777.

Philippine National REDD+ Strategy Team, Department of Environment and Natural Resources, & CoDe REDD-plus Philippines. (2011). Philippine National REDD+ Strategy.

Quegan, S., & Yu, J. J. (2001). Filtering of multichannel SAR images. IEEE Transactions on Geoscience and Remote Sensing, 39(11), 2373–2379.

Rodríguez-Veiga, P., Wheeler, J., Louis, V., Tansey, K., & Balzter, H. (2017). Quantifying Forest Biomass Carbon Stocks From Space. Current Forestry Reports, 3(1), 1–18.

Rouse, J. W., Haas, R. H., Schell, J. A., & Deering, D. W. (1974). Monitoring vegetation systems in the Great Plains with ERTS. ERTS-1 Symposium, 309–317.

Saatchi, S., Marlier, M., Chazdon, R. L., Clark, D. B., & Russell, A. E. (2011). Impact of spatial variability of tropical forest structure on radar estimation of aboveground biomass. Remote Sensing of Environment, 115(11), 2836–2849.

Santoro, M., & Cartus, O. (2018). Research Pathways of Forest Above-Ground Biomass Estimation Based on SAR Backscatter and Interferometric SAR Observations. Remote Sensing, 10(4), 608.

Schade, J., & Ludwig, R. (2013). Forest Carbon Baseline Study Leyte (p. 24) [Draft Report]. Deutsche Gesellschaft für Internationale Zusammenarbeit (GIZ) GmbH.

Shimada, M., Isoguchi, O., Tadono, T., & Isono, K. (2009). PALSAR radiometric and geometric calibration. IEEE Transactions on Geoscience and Remote Sensing, 47(12), 3915–3932.

Singh, M., Friess, D. A., Vilela, B., De Alban, J. D. T., Monzon, A. K. V., Veridiano, R. K. A., & Tumaneng, R. D. (2017). Spatial relationships between above-ground biomass and bird species biodiversity in Palawan, Philippines. PLOS ONE, 12(12), e0186742.

Sullivan, M. J. P., Talbot, J., Lewis, S. L., Phillips, O. L., Qie, L., Begne, S. K., Chave, J., Cuni-Sanchez, A., Hubau, W., Lopez-Gonzalez, G., Miles, L., Monteagudo-Mendoza, A., Sonké, B., Sunderland, T., ter Steege, H., White, L. J. T., Affum-Baffoe, K., Aiba, S., de Almeida, E. C., … Zemagho, L. (2017). Diversity and carbon storage across the tropical forest biome. Scientific Reports, 7(1).

Thapa, R. B., Watanabe, M., Motohka, T., & Shimada, M. (2015a). Potential of high-resolution ALOS–PALSAR mosaic texture for aboveground forest carbon tracking in tropical region. Remote Sensing of Environment, 160, 122–133.

Thapa, R. B., Watanabe, M., Motohka, T., Shiraishi, T., & Shimada, M. (2015b). Calibration of Aboveground Forest Carbon Stock Models for Major Tropical Forests in Central Sumatra Using Airborne LiDAR and Field Measurement Data. IEEE Journal of Selected Topics in Applied Earth Observations and Remote Sensing, 8(2), 661–673.

Thapa, R. B., Watanabe, M., Shimada, M., & Motohka, T. (2016). Examining High-Resolution PiSAR-L2 Textures for Estimating Tropical Forest Carbon Stocks. IEEE Journal of Selected Topics in Applied Earth Observations and Remote Sensing, 9(7), 3202–3209.

Tucker, C. J. (1979). Red and photographic infrared linear combinations for monitoring vegetation. Remote Sensing of Environment, 8(2), 127–150.

UNESCO World Heritage Centre. (2021, June 12). Northern Sierra Madre Natural Park and outlying areas inclusive of the buffer zone. UNESCO World Heritage Centre. https://whc.unesco.org/en/tentativelists/5037/

van Deventer, A. P., Ward, A. D., Gowda, P. H., & Lyon, J. G. (1997). Using Thematic Mapper data to identify contrasting soil plains and tillage practices. Photogrammetric Engineering & Remote Sensing, 63(1), 87–93.

Walker, S. M., Pearson, T. R. H., Casarim, F. M., Harris, N., Petrova, S., Grais, A., Swails, E., Netzer, M., Goslee, K. M., & Brown, S. (2012). Standard Operating Procedures for Terrestrial Carbon Measurement. Winrock International.

White, J. C., Wulder, M. A., Hobart, G. W., Luther, J. E., Hermosilla, T., Griffiths, P., Coops, N. C., Hall, R. J., Hostert, P., Dyk, A., & Guindon, L. (2014). Pixel-based image compositing for large-area dense time series applications and science. Canadian Journal of Remote Sensing, 40(3), 192–212.

Whitmore, T. C. (1984). Tropical Rain Forests of the Far East (2nd ed.). Clarendon Press.